Spin-Disorder-Induced Angular Anisotropy in Polarized Magnetic Neutron Scattering

Ivan Titov,[1] Mathias Bersweiler,[1] Michael P. Adams,[1] Evelyn Pratami Sinaga,[1,*] Venus Rai,[1] Štefan Liščák,[1] Max Lahr,[1] Thomas L. Schmidt,[1] Vladyslav M. Kuchkin,[1] Andreas Haller,[1] Kiyonori Suzuki,[2] Nina-Juliane Steinke,[3] Diego Alba Venero,[4] Dirk Honecker,[4] Joachim Kohlbrecher,[5] Luis Fernández Barquín,[6] and Andreas Michels[1,†]

[1]*Department of Physics and Materials Science, University of Luxembourg, 162A Avenue de la Faiencerie, 1511 Luxembourg, Grand Duchy of Luxembourg*

[2]*Department of Materials Science and Engineering, Monash University, Clayton, Victoria 3800, Australia*

[3]*Institute Laue-Langevin, 71 Avenue des Martyrs, 38042 Grenoble, France*

[4]*ISIS Neutron and Muon Facility, Rutherford Appleton Laboratory, Didcot OX110QX, United Kingdom*

[5]*Paul Scherrer Institute, CH-5232 Villigen PSI, Switzerland*

[6]*Department CITIMAC, Facultad de Ciencias, Universidad de Cantabria, 39005 Santander, Spain*

(Received 4 July 2025; revised 18 September 2025; accepted 23 October 2025; published 6 November 2025)

We experimentally report a hitherto unseen angular anisotropy in the polarized small-angle neutron scattering (SANS) cross section of a magnetically strongly inhomogeneous material. Based on an analytical prediction using micromagnetic theory, the difference between the spin-up and spin-down SANS cross sections is expected to show a spin-disorder-induced anisotropy. The effect is particularly pronounced in inhomogeneous magnetic materials, such as nanoporous ferromagnets, magnetic nanocomposites, or steels, which exhibit large nanoscale jumps in the saturation magnetization at internal pore-matrix or particle-matrix interfaces. Analysis of the experimental neutron data constitutes a method for determining the exchange-stiffness constant. Our results for the nuclear-magnetic interference terms contained in the polarized magnetic neutron scattering cross section might also be of relevance to other neutron techniques.

DOI: 10.1103/5yc2-pv4y

Introduction—Polarized neutron scattering is one of the most powerful techniques for investigating the structure and dynamics of condensed matter, in particular magnetic materials and superconductors [1,2]. Based on the seminal papers by Bloch [3,4], Schwinger [5], and Halpern and Johnson [6], the theory of polarized neutron scattering was worked out in the early 1960s by Maleev and Blume [7,8]. Several classic experimental studies [9–15] have demonstrated the basic principles and paved the way for today's three-dimensional cryogenic polarization-analysis device (CRYOPAD) [16–19]. With this technique it becomes possible to measure 16 correlation functions, which provide important information on the nuclear and magnetic structure of materials (see Refs. [20,21] for textbook expositions of polarized neutron scattering).

Compared to unpolarized neutrons, the scattering cross section for polarized neutrons contains additional contributions [22]. These are the familiar interference terms between the nuclear (structural) and magnetic scattering amplitudes and a purely magnetic-magnetic interference term (the so-called chiral function). In this Letter, we exclusively concentrate on the *nuclear-magnetic interference terms*. Based on an analytical prediction using the continuum theory of micromagnetics, more specifically for the transversal magnetization Fourier component [23], it is the central aim to experimentally search for the existence of a corresponding angular anisotropy in the nuclear-magnetic interference terms. This research makes a fundamental contribution to the understanding of polarized magnetic neutron scattering, and it widens the analysis capabilities of the polarized SANS technique by providing a method for determining the exchange constant.

We refer to Supplemental Material [24] for additional micromagnetic calculations supporting the experimental neutron data and for some basic structural and magnetic properties of the studied samples (see also Refs. [25–34] therein).

Experimental—The theoretical considerations (see below) require a polycrystalline magnetic material with strong nanoscale spatial variations in the saturation magnetization, i.e., $M_s = M_s(\mathbf{r})$. Therefore, for the neutron experiments, we used inert-gas condensed nanoporous Fe [26] and a melt-spun nanocrystalline $Fe_{89}Zr_7B_3Cu$ alloy (Nanoperm) [33]. The microstructure of the Fe sample consists of a distribution of nanosized pores in an Fe matrix, whereas the Nanoperm sample has a two-phase microstructure consisting of Fe nanoparticles that are embedded in an amorphous magnetic matrix of different magnetization. Hence, these specimens are characterized by large jumps ΔM in the magnitude of the saturation

*Present address: Department of Physics, Matana University, Gading Serpong, Tangerang, Banten 15810, Indonesia.

†Contact author: andreas.michels@uni.lu

magnetization at internal pore-matrix and particle-matrix interfaces, $\mu_0\Delta M \cong 2.15$ T for Fe and $\mu_0\Delta M \cong 1.5$ T for Nanoperm. The sample thicknesses for the SANS measurements were ∼500 μm (Fe) and ∼100 μm (Nanoperm). Unpolarized SANS investigations of these type of materials along with details regarding sample synthesis and microstructural and magnetic characterization can be found in Refs. [35–39].

The neutron experiment was conducted at the instrument D33 at the Institut Laue-Langevin, Grenoble, France [40,41]. We used an incident polarized neutron beam with a mean wavelength of $\lambda = 4.65$ Å and a wavelength broadening of $\Delta\lambda/\lambda = 10\%$ (full width at half maximum). Two sample-to-detector distances (13 and 5 m) allowed us to cover a q range of $0.04\ \mathrm{nm}^{-1} \lesssim q \lesssim 1.0\ \mathrm{nm}^{-1}$. The external magnetic field $\mathbf{H}_0$ was provided by a superconducting magnet ($\mu_0 H_0^{\max} = 3$ T) and applied perpendicular to the wave vector $\mathbf{k}_0$ of the incident neutron beam; see Fig. 1 for a schematic drawing of the experimental neutron setup. The beam was polarized by a magnetized FeSi multilayer mirror ($m = 3.6$), and an adiabatic resonance radio frequency (rf) spin flipper allowed us to reverse the initial neutron polarization. The flipping efficiency of the rf flipper was $\epsilon = 96\%$, and the polarization of the beam was $P = 98\%$ at $\lambda = 4.65$ Å. Further neutron experiments under similar conditions have been performed at the ZOOM beamline [42] at the ISIS Neutron and Muon Facility (Rutherford Appleton Laboratory, Didcot, United Kingdom) and at SANS-1 at the Paul Scherrer Institute (Villigen PSI, Switzerland). For SANS data reduction (correction for background scattering and polarization-dependent transmission), the GRASP software package was used [43].

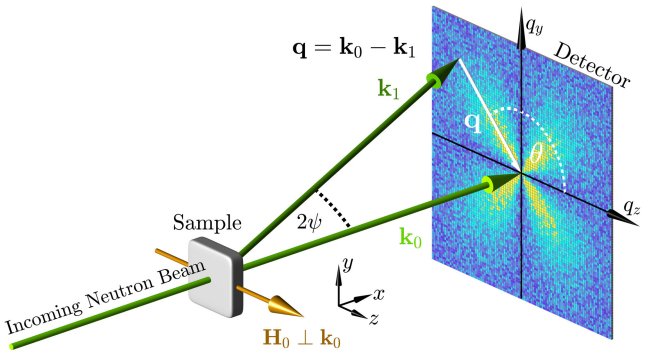

FIG. 1. Sketch of the neutron scattering geometry. The neutron optical elements (polarizer and spin flipper) that are required to measure the two spin-resolved SANS cross sections are not drawn. The applied magnetic field $\mathbf{H}_0 \| \mathbf{e}_z$ is perpendicular to the wave vector $\mathbf{k}_0 \| \mathbf{e}_x$ of the incident neutron beam ($\mathbf{H}_0 \perp \mathbf{k}_0$). The momentum-transfer or scattering vector $\mathbf{q}$ is defined as the difference between $\mathbf{k}_0$ and $\mathbf{k}_1$, i.e., $\mathbf{q} = \mathbf{k}_0 - \mathbf{k}_1$. The angle $\theta = \angle(\mathbf{q}, \mathbf{H}_0)$ is used to describe the angular anisotropy of the recorded scattering pattern on the two-dimensional detector.

Polarized SANS cross section—The focus in our Letter lies on the difference $\Delta\Sigma = d\Sigma^-/d\Omega - d\Sigma^+/d\Omega$ between the flipper-off ("−") and flipper-on ("+") SANS cross sections. Neglecting nuclear spin-dependent scattering and the chiral function, which is expected to average out for statistically isotropic polycrystalline magnetic materials, we can express $\Delta\Sigma$ as ($\mathbf{H}_0 \perp \mathbf{k}_0$, see Fig. 1) [44]

$$\Delta\Sigma = K[(\tilde{N}\tilde{M}_z^* + \tilde{N}^*\tilde{M}_z)\sin^2\theta - (\tilde{N}\tilde{M}_y^* + \tilde{N}^*\tilde{M}_y)\sin\theta\cos\theta], \quad (1)$$

where $K = (16\pi^3/V)b_{\mathrm{H}}$, V is the scattering volume, $b_{\mathrm{H}} = 2.91 \times 10^8\ \mathrm{A}^{-1}\ \mathrm{m}^{-1}$ is the magnetic scattering length in the small-angle regime (the atomic magnetic form factor is approximated by 1, since we are dealing with forward scattering), $\tilde{N}(\mathbf{q})$ and $\tilde{\mathbf{M}}(\mathbf{q}) = \{\tilde{M}_x, \tilde{M}_y, \tilde{M}_z\}$ denote, respectively, the Fourier transforms of the nuclear scattering-length density and of the magnetization vector field $\mathbf{M}(\mathbf{r}) = \{M_x, M_y, M_z\}$, θ is the angle between $\mathbf{H}_0 = H_0\mathbf{e}_z$ and $\mathbf{q}$, so that $\mathbf{q} \cong q\{0, \sin\theta, \cos\theta\}$ in small-angle approximation, and the asterisks "$*$" mark the complex-conjugated quantity.

Equation (1) shows that there are two nuclear-magnetic interference terms contributing to $\Delta\Sigma$ (in the $\mathbf{H}_0 \perp \mathbf{k}_0$ geometry): for isotropic $\tilde{N}$ and $\tilde{M}_z$, the first term exhibits the well-known $\sin^2\theta$ anisotropy, which has been observed countless times in polarized SANS experiments. It is the central aim of this Letter to report on the experimental first-time observation of the second scattering term in Eq. (1), which allows the direct measurement of the exchange-stiffness constant. As we will detail in the following, this is accomplished in strongly inhomogeneous (regarding the spatial variation of the saturation magnetization) nanoporous Fe [26] and in the two-phase nanocrystalline alloy Nanoperm [36].

Micromagnetic SANS theory—Theory predicts that in the two-dimensional y-z detector plane (see Fig. 1) the transversal magnetization Fourier component $\tilde{M}_y = \tilde{M}_y(q_x = 0, q_y, q_z)$ takes on the following form [45]:

$$\tilde{M}_y = \frac{p(\tilde{H}_{\mathrm{py}} - \tilde{M}_z\sin\theta\cos\theta)}{1 + p\sin^2\theta}, \quad (2)$$

where $\tilde{H}_{\mathrm{py}}$ denotes the Cartesian component of the Fourier transform of the magnetic anisotropy field, $\tilde{M}_z$ is the longitudinal magnetization Fourier component, and $p(q, H_0) = M_0/[H_0(1 + l_{\mathrm{H}}^2 q^2)]$ is a known dimensionless function of q and H_0, where $l_{\mathrm{H}}(H_0) = [2A/(\mu_0 M_0 H_0)]^{1/2}$ denotes the micromagnetic exchange length of the field; A is the exchange-stiffness constant, and $M_0 = \langle M_{\mathrm{s}}(\mathbf{r})\rangle$ denotes the macroscopic saturation magnetization of the sample, which corresponds to the spatial average ($\langle\ldots\rangle$) of $M_{\mathrm{s}}(\mathbf{r})$. Equation (2) results from the micromagnetic theory

of the magnetic SANS cross section of bulk ferromagnets, which takes into account the isotropic exchange interaction, magnetic anisotropy, the magnetodipolar interaction, as well as the external magnetic field [46].

If we assume that the nuclear scattering amplitude is isotropic, $\tilde{N} = \tilde{N}(q)$, and that $\tilde{H}_{py}$ varies randomly in the plane perpendicular to $\mathbf{H}_0 \| \mathbf{e}_z$ (equal number of "up" and "down" orientations of $\tilde{H}_{py}$ in a statistically isotropic sample), then the corresponding averages over the direction of the anisotropy field vanish [47]. The $\tilde{N}\tilde{M}_y$ scattering contribution in Eq. (1) is then given by

$$2\tilde{N}\tilde{M}_y \sin\theta\cos\theta = -\frac{2p\tilde{N}\tilde{M}_z \sin^2\theta\cos^2\theta}{1 + p\sin^2\theta}, \qquad (3)$$

where we have further assumed that $\tilde{N}$, $\tilde{M}_y$, and $\tilde{M}_z$ are real-valued functions. Note the dominant angular $\sin^2\theta\cos^2\theta$ anisotropy of this term. Since $\tilde{M}_z(q)$ represents, in the approach-to-saturation regime, the Fourier transform of the saturation magnetization profile $M_s(r)$ of the sample, it is directly seen that the $\sin^2\theta\cos^2\theta$ contribution is expected to be observed for strongly inhomogeneous materials such as magnetic nanocomposites or porous ferromagnets [on top of the $\sin^2\theta$ anisotropy; compare Eq. (1)]. On the other hand, when M_s = constant throughout the sample, as is appropriate for homogeneous single-phase magnets, the corresponding scattering only shows up at the origin of reciprocal space and cannot be observed. We emphasize that both $\tilde{M}_y$ and $\tilde{M}_z$ depend on the applied field H_0, but that $\tilde{M}_y$ tends to zero as $H_0 \to \infty$, while $\tilde{M}_z$ takes on its maximum value ($\tilde{M}_s$) in this limit. Therefore, in addition to their different angular anisotropies, field-dependent experiments are key to unraveling the two contributions to Eq. (1).

Inserting Eq. (3) into Eq. (1) we obtain for the difference cross section

$$\Delta\Sigma = 2K\tilde{N}\tilde{M}_z \sin^2\theta\left[1 + \frac{p\cos^2\theta}{1 + p\sin^2\theta}\right]. \qquad (4)$$

Figure 1 in Supplemental Material [24] displays the two-dimensional $\Delta\Sigma = \Delta\Sigma(q, \theta, H_0)$ [Eq. (4)] at a series of applied magnetic fields. There, it is seen that overall a $\sin^2\theta$ type angular anisotropy prevails in the data at all fields and that with decreasing H_0 the pattern broadens.

Finally, subtracting the saturated term ($\propto \sin^2\theta$) in Eq. (4) yields the field-dependent contribution

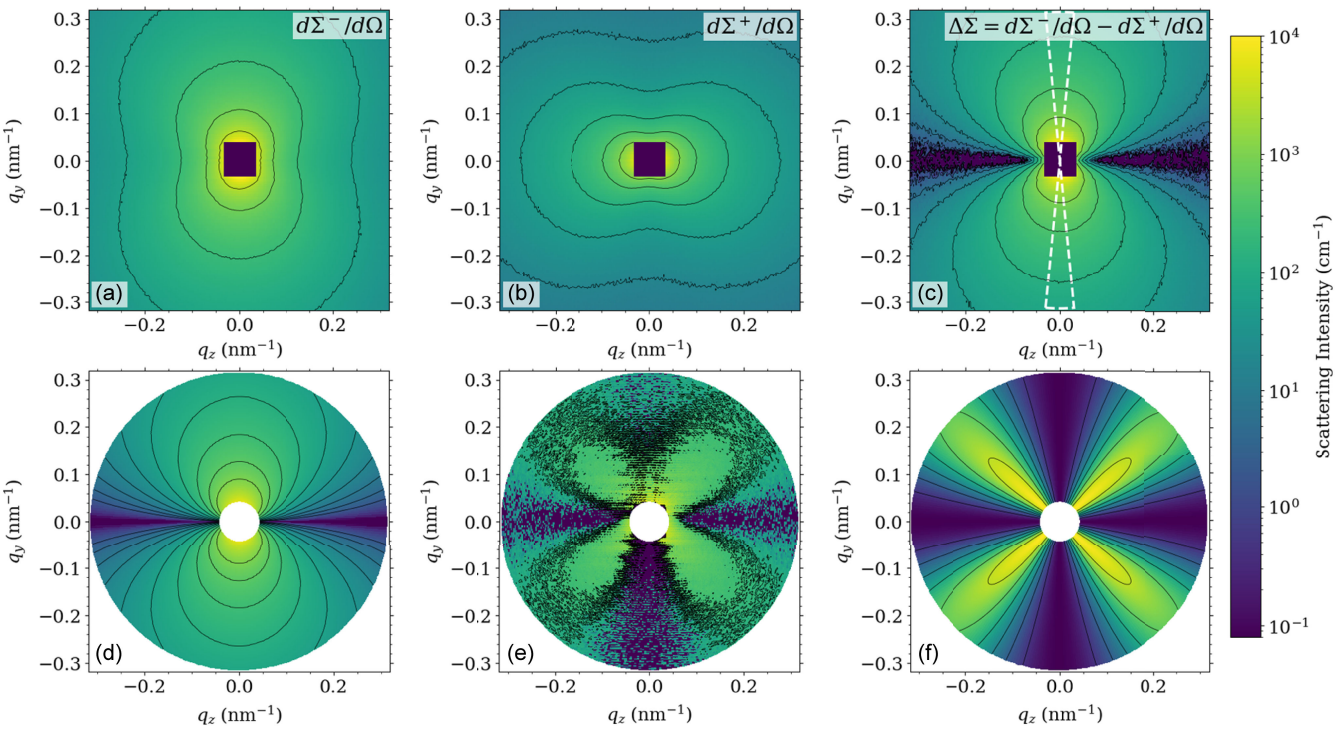

FIG. 2. Neutron data analysis procedure. (a) $d\Sigma^-/d\Omega$, (b) $d\Sigma^+/d\Omega$, and (c) $\Delta\Sigma = d\Sigma^-/d\Omega - d\Sigma^+/d\Omega$ of inert-gas condensed (igc) nanoporous Fe ($\mu_0 H_0 = 3.0$ T). (d) $\Delta\Sigma_{\theta=90°}\sin^2\theta$ extrapolated on the 2D detector using the $\Delta\Sigma$ data along the vertical direction from (c) (indicated by the white dashed lines). The data set shown in (d) corresponds to the first term in Eq. (4). (e) Difference between the experimental data (c) and the extrapolated contribution (d). Note that subfigures (a)–(e) show experimental data, while (f) features the analytical micromagnetic result for $\Delta\Sigma_H$ [Eq. (5)]. Materials parameters for Fe were used [24].

$$\Delta\Sigma_{\mathrm{H}} = 2K\tilde{N}\tilde{M}_z \frac{p\sin^2\theta\cos^2\theta}{1+p\sin^2\theta}, \tag{5}$$

which represents the main analytical result of this Letter. Straightforward analysis shows that the maxima $\theta_{\max}$ of Eq. (5) shift from about 45° at high fields (small p) to about 30° at low fields (large p) [24]. This provides a clear pathway towards identifying the angular anisotropy under question in experimental neutron data. We note that a particle-size distribution is not explicitly taken into account in the micromagnetic analysis; it would need to be included into the expressions for the nuclear scattering amplitude $\tilde{N}$ and for the longitudinal Fourier component $\tilde{M}_z$ contained in Eq. (5). This can only be accomplished numerically and is beyond the scope of the present Letter.

Experimental results and discussion—The experimental data analysis procedure is explained in Fig. 2 and the polarized neutron results are summarized in Fig. 3. For the case of inert-gas condensed nanoporous Fe at an applied magnetic field of $\mu_0 H_0 = 3$ T, we show in Figs. 2(a) and 2(b) the two half-polarized SANS cross sections $d\Sigma^-/d\Omega$ and $d\Sigma^+/d\Omega$, while the difference $\Delta\Sigma = d\Sigma^-/d\Omega - d\Sigma^+/d\Omega$ is displayed in Fig. 2(c). At an angle of $\theta = 90°$ [see the white dashed lines in Fig. 2(c)], the second term in Eq. (4) vanishes and we obtain the "usual" nuclear-magnetic interference term $\Delta\Sigma_{\theta=90°} = 2K\tilde{N}\tilde{M}_z$. This contribution depends on the magnitude q of the scattering vector, and under the assumption that both amplitudes $\tilde{N}$ and $\tilde{M}_z$ are isotropic (i.e., θ independent), we can generate (extrapolate) the corresponding 2D contribution $\Delta\Sigma_{\theta=90°}\sin^2\theta$ to Eq. (4) [Fig. 2(d)]. These 2D data are then subtracted from the experimental $\Delta\Sigma$ data [Fig. 2(c)] to approximately obtain the $\Delta\Sigma_{\mathrm{H}}$ term of Eq. (5) [Figs. 2(e) and 2(f)]. In this way we unravel the dominant $\sin^2\theta\cos^2\theta$ type angular anisotropy of interest.

The $\sin^2\theta\cos^2\theta$ type angular anisotropy is also observed in the nanoporous Fe sample at a lower field of 0.1 T [Fig. 3(a)] and also becomes visible in the polarized SANS data of the two-phase alloy Nanoperm at 3 T [Fig. 3(b)]. In Nanoperm, the anisotropy is less pronounced, which might be related to the fact that the jump in the saturation magnetization in this material is smaller than in the igc Fe sample. We also emphasize that for the field regime studied here both samples are within the approach-to-saturation regime [24].

Figure 3(c) displays the angular variation of $\Delta\Sigma_{\mathrm{H}}$ of inert-gas condensed Fe at a field of 0.1 T and for $q = 0.22$ nm^{-1}. The solid line in Fig. 3(c) represents a fit to Eq. (5) with two free parameters: the product $2K\tilde{N}\tilde{M}_z$ is assumed to be constant at a fixed q value ($2K\tilde{N}\tilde{M}_z = 39.9 \pm 9.8$ cm^{-1}) and the exchange-stiffness constant A in the function p is obtained as $A = (5.1 \pm 0.2) \times 10^{-11}$ J/m. The latter value, which represents an average over the sample volume, is a factor of about two larger than experimental A values for single crystalline Fe [48], a finding that requires further studies on defect-rich inert-gas condensed samples.

Conclusion—We have theoretically predicted and experimentally verified the existence of a spin-disorder-induced angular anisotropy in the polarized magnetic small-angle neutron scattering cross section. In the approach-to-saturation regime, the result Eq. (5) is of general relevance to magnetically inhomogeneous materials, such as nanoporous magnets, nanocomposites and permanent magnets, or steels, which exhibit a strong variation in the saturation magnetization $M_s(\mathbf{r})$. Analysis of the angular dependence of $\Delta\Sigma_{\mathrm{H}}$ provides a means to determine the exchange constant. Since the nuclear-magnetic interference term under question ($\propto \tilde{N}\tilde{M}_y$) is generically contained in the polarized neutron scattering cross section it is of interest to verify its existence with other techniques such as neutron diffraction. Likewise, polarized SANS experiments on a series of stepwise annealed samples could provide further information on the spin-disorder-induced angular anisotropy. Careful annealing (to avoid a too strong coarsening of the microstructure) may lead to the gradual

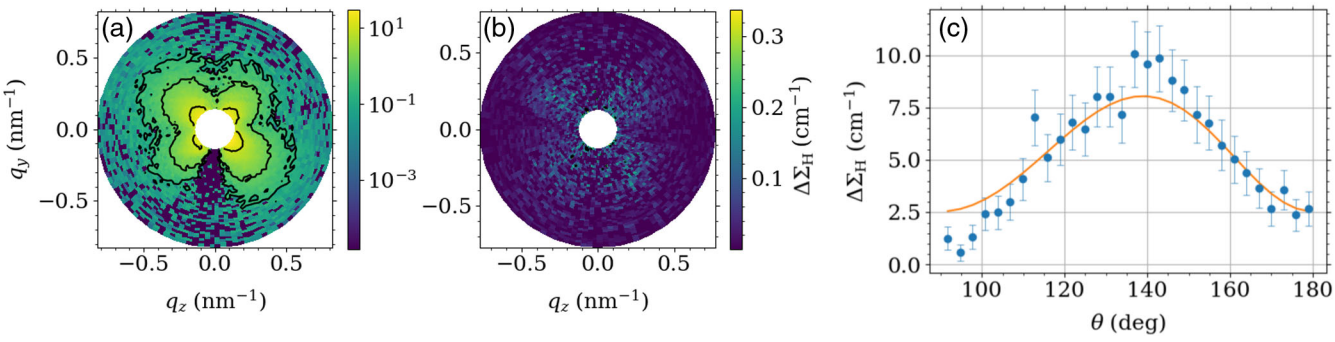

FIG. 3. Experimental polarized SANS results of inert-gas condensed (igc) nanoporous Fe and nanocrystalline $Fe_{89}Zr_7B_3Cu$ alloy (Nanoperm). (a) $\Delta\Sigma_{\mathrm{H}}$ of igc Fe at 0.1 T; (b) $\Delta\Sigma_{\mathrm{H}}$ of Nanoperm at 3.0 T; (c) (•) Experimental $\Delta\Sigma_{\mathrm{H}}(\theta)$ of igc Fe at 0.1 T, $q = 0.22$ nm^{-1}, and for $90° \lesssim \theta \lesssim 180°$ [upper left quadrant in (a)]. Solid line: fit to Eq. (5).

homogenization of the microstructure and in the concomitant reduction of mesoscale spin disorder, in which case the anisotropy is expected to vanish.

Acknowledgments—M. P. A., E. P. S., Š. L., V. M. K., A. H., T. L. S., and A. M. acknowledge financial support from the National Research Fund of Luxembourg (PRIDE MASSENA Grant, AFR Grants No. 15639149, No. AFR/23/17951349, and DeQuSky Grant No. C22/MS/17415246). V. M. K. acknowledges financial support from the European Union's Horizon 2020 research and innovation program under the Marie Skłodowska-Curie Grant Agreement No. 101203692 (QUANTHOPF). L. F. B. acknowledges project PID2023-146448OB. Moreover, the authors thank the Science and Technology Facilities Council at ISIS, the Swiss spallation neutron source at the Paul Scherrer Institute, and the Institut Laue-Langevin for the provision of neutron beam time.

Data availability—The data that support the findings of this article are not publicly available. The data are available from the authors upon reasonable request.

[1] T. Chatterji, *Neutron Scattering from Magnetic Materials* (Elsevier, Amsterdam, 2006).
[2] A. T. Boothroyd, *Principles of Neutron Scattering from Condensed Matter* (Oxford University Press, Oxford, 2020).
[3] F. Bloch, On the magnetic scattering of neutrons, Phys. Rev. **50**, 259 (1936).
[4] F. Bloch, On the magnetic scattering of neutrons. II, Phys. Rev. **51**, 994 (1937).
[5] J. S. Schwinger, On the magnetic scattering of neutrons, Phys. Rev. **51**, 544 (1937).
[6] O. Halpern and M. H. Johnson, On the magnetic scattering of neutrons, Phys. Rev. **55**, 898 (1939).
[7] S. V. Maleev, V. G. Bar'yakhtar, and R. A. Suris, The scattering of slow neutrons by complex magnetic structures, Sov. Phys. Solid State **4**, 2533 (1963).
[8] M. Blume, Polarization effects in the magnetic elastic scattering of slow neutrons, Phys. Rev. **130**, 1670 (1963).
[9] C. G. Shull, E. O. Wollan, and W. C. Koehler, Neutron scattering and polarization by ferromagnetic materials, Phys. Rev. **84**, 912 (1951).
[10] R. M. Moon, T. Riste, and W. C. Koehler, Polarization analysis of thermal-neutron scattering, Phys. Rev. **181**, 920 (1969).
[11] M. Th. Rekveldt, Neutron depolarisation as a method to determine the magnetization, the mean domain size and the mean square components of the inner magnetization of ferromagnets, J. Phys. (Paris), Colloq. **32**, C1 (1971).
[12] G. M. Drabkin, A. I. Okorokov, and V. V. Runov, Anisotroy of depolarization of a neutron beam, JETP Lett. **15**, 324 (1972).
[13] A. I. Okorokov, V. V. Runov, and A. G. Gukasov, Three-dimensional neutron polarimeter and spin dynamics investigation, Nucl. Instrum. Methods **157**, 487 (1978).
[14] F. Mezei, La nouvelle vague in polarized neutron scattering, Physica (Amsterdam) **137B**, 295 (1986).
[15] O. Schärpf and H. Capellmann, The *XYZ*-difference method with polarized neutrons and the separation of coherent, spin incoherent, and magnetic scattering cross sections in a multidetector, Phys. Status Solidi A **135**, 359 (1993).
[16] F. Tasset, Zero field neutron polarimetry, Physica (Amsterdam) **156–157B**, 627 (1989).
[17] P. J. Brown, J. B. Forsyth, and F. Tasset, Neutron polarimetry, Proc. R. Soc. A **442**, 147 (1993).
[18] F. Tasset, P. J. Brown, E. Lelièvre-Berna, T. Roberts, S. Pujol, J. Alibon, and E. Bourgeat-Lami, Spherical neutron polarimetry with Cryopad-II, Physica (Amsterdam) **267–268B**, 69 (1999).
[19] A. I. Okorokov and V. V. Runov, Vector analysis of polarization at small-angle neutron scattering, Physica (Amsterdam) **297B**, 239 (2001).
[20] W. G. Williams, *Polarized Neutrons* (Clarendon Press, Oxford, 1988).
[21] S. W. Lovesey, *Theory of Neutron Scattering from Condensed Matter*, Vol. I and II (Clarendon Press, Oxford, 1984).
[22] S. V. Maleev, Polarized neutron scattering in magnets, Phys. Usp. **45**, 569 (2002).
[23] A. Michels, D. Mettus, D. Honecker, and K. L. Metlov, Effect of Dzyaloshinski-Moriya interaction on elastic small-angle neutron scattering, Phys. Rev. B **94**, 054424 (2016).
[24] See Supplemental Material at http://link.aps.org/supplemental/10.1103/5yc2-pv4y for further details on the analytical micromagnetic SANS theory and for some structural and magnetic properties of the studied samples.
[25] D. Michels, C. E. Krill III, and R. Birringer, Grain-size-dependent Curie transition in nanocrystalline Gd: The influence of interface stress, J. Magn. Magn. Mater. **250**, 203 (2002).
[26] A. Michels, M. Elmas, F. Döbrich, M. Ames, J. Markmann, M. Sharp, H. Eckerlebe, J. Kohlbrecher, and R. Birringer, Porosity-induced spin disorder in nanocrystalline inert-gas-condensed iron, Europhys. Lett. **85**, 47003 (2009).
[27] C. E. Krill and R. Birringer, Estimating grain-size distributions in nanocrystalline materials from X-ray diffraction profile analysis, Philos. Mag. A **77**, 621 (1998).
[28] J. C. H. Shih, L. Bourgeois, K. Suzuki, and J. S. Garitaonandia, Grain growth process of two-phase nanocrystalline soft magnetic materials, J. Magn. Magn. Mater. **304**, e693 (2006).
[29] G. Herzer, Nanocrystalline Soft magnetic alloys, in *Handbook of Magnetic Materials*, Vol. 10, edited by K. H. J. Buschow (Elsevier, Amsterdam, 1997), pp. 415–462.
[30] G. Herzer, Modern soft magnets: Amorphous and nanocrystalline materials, Acta Mater. **61**, 718 (2013).
[31] Z. Li, R. Parsons, B. Zang, H. Kishimoto, T. Shoji, A. Kato, J. Karel, and K. Suzuki, Dramatic grain refinement and magnetic softening induced by Ni addition in FeB based nanocrystalline soft magnetic alloys, Scr. Mater. **181**, 82 (2020).
[32] F. Carmona, V. Madurga, and M. Vázquez, Approach to magnetic saturation in $(Co_{0.95}Fe_{0.05})_{75}Si_{15}B_{10}$ amorphous alloy, J. Magn. Magn. Mater. **62**, 68 (1986).
[33] A. Michels, C. Vecchini, O. Moze, K. Suzuki, J. M. Cadogan, P. K. Pranzas, and J. Weissmüller, Dipole-field-induced spin disorder in a nanocomposite soft magnet, Europhys. Lett. **72**, 249 (2005).

[34] K. Suzuki, A. Makino, A. Inoue, and T. Masumoto, Low core losses of nanocrystalline Fe-M-B (M = Zr, Hf, or Nb) alloys, J. Appl. Phys. **74**, 3316 (1993).

[35] A. Michels, R. N. Viswanath, and J. Weissmüller, Domain formation and long-range spin disorder in Vitroperm, Europhys. Lett. **64**, 43 (2003).

[36] A. Michels, C. Vecchini, O. Moze, K. Suzuki, P. K. Pranzas, J. Kohlbrecher, and J. Weissmüller, Dipolar correlations in a nanocomposite: A neutron scattering study of Nanoperm $Fe_{89}Zr_7B_3Cu$, Phys. Rev. B **74**, 134407 (2006).

[37] F. Döbrich, J. Kohlbrecher, M. Sharp, H. Eckerlebe, R. Birringer, and A. Michels, Neutron scattering study of the magnetic microstructure of nanocrystalline gadolinium, Phys. Rev. B **85**, 094411 (2012).

[38] M. Bersweiler, M. P. Adams, I. Peral, J. Kohlbrecher, K. Suzuki, and A. Michels, Unraveling the magnetic softness in Fe–Ni–B-based nanocrystalline material by magnetic small-angle neutron scattering, IUCrJ **9**, 65 (2022).

[39] V. Rai, I. Titov, M. P. Adams, K. Suzuki, J. Kohlbrecher, and A. Michels, Magnetic microstructure of nanocrystalline Fe-Nb-B alloys as seen by small-angle neutron and x-ray scattering, Phys. Rev. B **110**, 054437 (2024).

[40] C. D. Dewhurst, I. Grillo, D. Honecker, M. Bonnaud, M. Jacques, C. Amrouni, A. Perillo-Marcone, G. Manzin, and R. Cubitt, The small-angle neutron scattering instrument D33 at the Institut Laue-Langevin, J. Appl. Crystallogr. **49**, 1 (2016).

[41] M. Bersweiler, M. P. Adams, D. Alba Venero, D. Honecker, A. Michels, S. Mühlbauer, E. Pratami Sinaga, N.-J. Steinke, and I. Titov, Novel angular anisotropy in polarized SANS, Proposal number: DIR-272, Institut Laue-Langevin (2023), 10.5291/ILL-DATA.DIR-272.

[42] M. Bersweiler, M. P. Adams, E. Pratami Sinaga, I. Titov, D. Alba Venero, D. Honecker, and A. Michels, Novel angular anisotropy in polarized SANS, STFC ISIS Neutron and Muon Source, 10.5286/ISIS.E.RB2220057-1.

[43] C. D. Dewhurst, Graphical reduction and analysis small-angle neutron scattering program: GRASP, J. Appl. Crystallogr. **56**, 1595 (2023).

[44] A. Michels, *Magnetic Small-Angle Neutron Scattering: A Probe for Mesoscale Magnetism Analysis* (Oxford University Press, Oxford, 2021).

[45] This expression for $\tilde{M}_y$ follows from Eq. (25) in Ref. [23] by setting the Dzyaloshinskii-Moriya interaction length equal to zero ($l_D = 0$), assuming the scattering geometry where the applied magnetic field is perpendicular to the incident neutron beam ($q_x = 0$), and noting that $\tilde{M}_z = M_s \tilde{I}_m$, $q_y q_z/q^2 = \sin\theta\cos\theta$, and $q_y^2/q^2 = \sin^2\theta$ (in the notation of Ref. [23]).

[46] Equation (2) is valid in the approach-to-saturation regime, when the governing micromagnetic expressions can be linearized. For a detailed derivation, see Ref. [23], which considers the effect of the Dzyaloshinskii-Moriya interaction on the elastic magnetic SANS cross section and the chiral function.

[47] A statistically isotropic polycrystalline magnetic material may be characterized by random variations of the magnitude and direction of the magnetic anisotropy field, e.g., from one crystallite to another. In our experiment, a large external magnetic field is applied, which gives rise to a longitudinal (z) magnetization component that is close to the saturation value. For this scenario, the expectation values of the two transversal components of the anisotropy field vanish. Consequently, when averaging the $\tilde{N}\tilde{M}_y$ term in Eq. (1) [using Eq. (2)] over the directions of the anisotropy field, the $\tilde{N}\tilde{H}_{py}$ term vanishes, and only the averages over $\tilde{N}\tilde{M}_z$ remain.

[48] H. Kronmüller and M. Fähnle, *Micromagnetism and the Microstructure of Ferromagnetic Solids* (Cambridge University Press, Cambridge, 2003).